



HAL
open science

Visible and near-infrared nightglow of molecular oxygen in the atmosphere of Venus

A. García Muñoz, Franklin P. Mills, T. G. Slanger, Giuseppe Piccioni, Pierre
Drossart

► **To cite this version:**

A. García Muñoz, Franklin P. Mills, T. G. Slanger, Giuseppe Piccioni, Pierre Drossart. Visible and near-infrared nightglow of molecular oxygen in the atmosphere of Venus. *Journal of Geophysical Research. Planets*, 2009, 114, pp.12002. 10.1029/2009JE003447 . hal-03742763

HAL Id: hal-03742763

<https://hal.science/hal-03742763>

Submitted on 5 Sep 2022

HAL is a multi-disciplinary open access archive for the deposit and dissemination of scientific research documents, whether they are published or not. The documents may come from teaching and research institutions in France or abroad, or from public or private research centers.

L'archive ouverte pluridisciplinaire **HAL**, est destinée au dépôt et à la diffusion de documents scientifiques de niveau recherche, publiés ou non, émanant des établissements d'enseignement et de recherche français ou étrangers, des laboratoires publics ou privés.

Visible and near-infrared nightglow of molecular oxygen in the atmosphere of Venus

A. García Muñoz,^{1,2} F. P. Mills,^{1,3} T. G. Slanger,⁴ G. Piccioni,⁵
and P. Drossart⁶

Received 1 June 2009; revised 20 August 2009; accepted 31 August 2009; published 23 December 2009.

[1] The Herzberg II system of O₂ has been a known feature of Venus' nightglow since the Venera 9 and 10 orbiters detected its $c(0)-X(v'')$ progression more than 3 decades ago. We search for its emission at 400 nm–700 nm in spectra obtained with the VIRTIS instrument on Venus Express. Despite the weakness of the signal, integration over a few hours of limb observations of the planet's upper atmosphere reveals the unambiguous pattern of the progression. The selected data sample mainly the northern latitudes within a few hours of local midnight. The emission is ubiquitous on the nightside of Venus and can be discerned at tangent altitudes from 80 km to 110 km. The average emission vertical profiles of the $c(0)-X(v'')$ progression and the O₂ $a(0)-X(0)$ band, the latter from simultaneous near-infrared spectra, are quite similar, with their respective peaks occurring within ± 1 km of each other. We conclude that the net yield for production of the $c(0)$ state is low, $\sim 1\%$ – 2% of the oxygen recombination rate, and that O(³P) and CO₂ are the two likely quenchers of the Herzberg II nightglow, although CO cannot be ruled out. We also derive a value of $2.45 \times 10^{-16} \text{ cm}^3 \text{ s}^{-1}$ for the rate constant at which CO₂ collisionally quenches the $c(0)$ state. Our VIRTIS spectra show hints of O₂ $A'(0)-a(v'')$ emission but no traces of the O (¹S–¹D) green line at 557.7 nm.

Citation: García Muñoz, A., F. P. Mills, T. G. Slanger, G. Piccioni, and P. Drossart (2009), Visible and near-infrared nightglow of molecular oxygen in the atmosphere of Venus, *J. Geophys. Res.*, 114, E12002, doi:10.1029/2009JE003447.

1. Introduction

[2] The remote spectrum of Venus' nightside from middle-ultraviolet to near-infrared wavelengths shows evidence of nightglow emission from O₂, NO, O(¹S) and OH [Krasnopolsky *et al.*, 1977; Feldman *et al.*, 1979; Slanger *et al.*, 2001; Piccioni *et al.*, 2008]. The O(³P) atom, which plays an essential role in the photochemistry of the planet's atmosphere [Mills *et al.*, 2006; Mills and Allen, 2007], is a fundamental ingredient in the production of these emissions. The origin of the O₂ nightglow can be unequivocally traced to oxygen atoms, which makes the emission from O₂ a particularly interesting target in the investigation of Venus' upper atmosphere.

[3] The O₂ $a(0)-X(0)$ band at 1.27 μm is the strongest feature in Venus' nightglow. It has been studied from both ground-based facilities and space platforms [Connes *et al.*,

1979; Drossart *et al.*, 1993]. A typical hemispheric average zenith intensity for the so-called O₂ IR Atmospheric Band is 1 MegaRayleigh, although it can vary drastically over hours to days [Crisp *et al.*, 1996]. The variability is attributed to the rapidly evolving conditions of Venus' upper atmospheric winds. As illustrated extensively by ground-based observations [Ohtsuki *et al.*, 2005, 2008a, 2008b; Bailey *et al.*, 2008a, 2008b], the brightest emission is most likely to originate in the vicinity of the antisolar point, an indication that the oxygen atoms that recombine to produce the $a(0)-X(0)$ band are transported by the subsolar-to-antisolar circulation of Venus' upper atmosphere.

[4] The $a(0)-X(0)$ band was not the first Venusian O₂ nightglow emission reported. In the mid-1970s, the spectrometers on the Venera 9 and 10 orbiters recorded an emission pattern at visible wavelengths as the line of sight of the instrument grazed the upper layers of the atmosphere [Krasnopolsky *et al.*, 1977]. The pattern was correctly assigned to the O₂ $c(0)-X(v'')$ progression by Lawrence *et al.* [1977], who produced a spectrum similar to that of the Veneras from an oxygen discharge flow experiment in which carbon dioxide was added downstream of the discharge to simulate the bulk composition of Venus' atmosphere. A later experiment confirmed the assignment [Slanger, 1978] and, further, identified a few weak O₂ $A'(0)-a(v'')$ bands in the Venera spectra [Slanger and Black, 1978]. The $c-X$ and $A'-a$ transitions of O₂ are often referred to, respectively, as the Herzberg II and Chamberlain systems of that molecule. After conversion into zenith

¹Research School of Physics and Engineering, Australian National University, Canberra, ACT, Australia.

²Now at the Instituto de Astrofísica de Canarias, La Laguna, Spain.

³Fenner School of Environment and Society, Australian National University, Canberra, ACT, Australia.

⁴Molecular Physics Laboratory, SRI International, Menlo Park, California, USA.

⁵Istituto di Astrofisica Spaziale e Fisica Cosmica, Rome, Italy.

⁶LESIA, Observatoire de Paris, UPMC, Université Paris-Diderot, CNRS, Meudon, France.

intensities, *Krasnopolsky* [1983] quotes an emission intensity of 2–3 kR for the entire $c(0)–X(v'')$ progression in the Venera measurements and about 15 times less for $A'(0)–a(v'')$. Years later, *Bougher and Borucki* [1994] observed with the star tracker on the Pioneer Venus Orbiter (PVO) a visible spectrally unresolved brightness that was ascribed to the Herzberg II system. More recently, *Slanger et al.* [2001, 2006] have resolved a few rotational lines in the 0–10 Herzberg II band near 550 nm in observations with the Keck I and Apache Point Observatory telescopes. The intensities reported by *Bougher and Borucki* [1994] and *Slanger et al.* [2001, 2006] are in reasonable accord with those from the Venera missions.

[5] The O₂ nightglow has never been observed on Mars, although the Martian atmosphere contains the oxygen and carbon dioxide that are essential to Venus' O₂ nightglow. On Earth, the record of observed O₂ nightglow emissions is quite extensive and includes transitions from the A , A' , c , b and a electronic states and a dense array of vibrational v' and v'' levels [*Slanger and Copeland*, 2003; *Cosby et al.*, 2006]. The appearance of the terrestrial O₂ nightglow spectrum is richer and bluer than that of its Venusian counterpart. As a number of laboratory experiments have demonstrated [*Lawrence et al.*, 1977; *Slanger*, 1978; *Kenner et al.*, 1979; *Kenner and Ogryzlo*, 1983; *Stott and Thrush*, 1989; *Steadman and Thrush*, 1994; *Slanger and Copeland*, 2003], the difference stems from the distinct ways in which the major atmospheric constituents, O₂/N₂ on Earth and CO₂ on Venus, collisionally relax the excited oxygen molecules. Polyatomic molecules have more modes of vibration than diatomic molecules, which opens different pathways for energy transfer between them and the excited O₂ molecule. In the case of CO₂, this seems to favor the production of the $c(0)$ and $A'(0)$ states.

[6] On Earth, there is a correlation between the intensities of the O₂ nightglow and the green line of atomic oxygen that occurs in the $O(^1S–^1D)$ transition at 557.7 nm [*Slanger et al.*, 2004]. No connection has been demonstrated yet for Venus, but the recent discovery of the green line [*Slanger et al.*, 2001] has prompted a renewed interest in the electronically excited forms of molecular oxygen in the Venusian atmosphere.

[7] Near-infrared spectra collected with the Visible and Infrared Thermal Imaging Spectrometer (VIRTIS) on Venus Express have been found to contain the 0–0 and 0–1 bands of O₂ $a–X$, the 1–0, 2–1, 2–0 and 3–2 bands of OH $X–X$ and the 0–0 band of NO $C–A$, all of them except the O₂ band at 1.27 μm seen for the first time in the atmosphere of Venus [*Piccioni et al.*, 2008; *García Muñoz et al.*, 2009]. In the present work, we extend the investigation of Venus' nightglow with VIRTIS to the visible wavelengths, where the O₂ $c(0)–X(v'')$ progression appears as a prominent emission.

2. Observations

2.1. Data Collection and Calibration

[8] VIRTIS-M is the double-channel mapping spectrometer of the VIRTIS instrument on Venus Express [*Piccioni et al.*, 2009a]. The visible and infrared channels of VIRTIS-M provide moderate-resolution spectroscopy ($\lambda/\Delta\lambda \sim 100–200$) over 432 spectral bands each, for wavelengths ranging

from 0.3 to 1.1 μm and from 1 to 5 μm , respectively. The instrument's telescope is boresighted toward a permanent direction in the inertial frame of the spacecraft. With the scanning mirror fixed, the instantaneous field of view (IFOV) of the instrument is $0.25 \times 64 \text{ mrad}^2$, or $0.25 \times 0.25 \text{ mrad}^2$ for each of the 256 pixels along the slit. The absolute pointing accuracy of each pixel is much better than that [*Piccioni et al.*, 2009b].

[9] Venus Express revolves in an eccentric, 24-h orbit around Venus. Periapsis occurs at $\sim 80^\circ\text{N}$, as the spacecraft passes about 300 km above the surface of the planet. From near periapsis, the narrow field of view of the instrument makes it possible to obtain high spatial resolution, limb-viewing spectra of Venus' northern hemisphere. This observing configuration is excellent for studying weak emission signatures in the planet's upper atmosphere.

[10] For an IFOV of 0.25 mrad, the vertical resolution on the planet's limb that can be achieved in a single exposure from a typical distance for limb observations of a few thousand kilometers is of only a few kilometers or less. Pointing uncertainties partially cancel out when multiple observations are summed up. Thus, it is possible to have vertical resolutions better than 1 km by grouping a few hundreds of observations from a common tangent altitude.

[11] For our analysis, we have collected only limb-viewing sessions with exposure times of 8 s for both VIRTIS-M channels. The data were acquired over 41 orbits between January 2007 and May 2008. Overall, we have more than 2×10^5 spectra of Venus' atmosphere for altitudes at the tangent point between 80 and 110 km. The total exposure time amounts to about 450 h. Unlike the $a(0)–X(0)$ band, identification with VIRTIS-M of the much weaker $c(0)–X(v'')$ progression is very sensitive to the total exposure time. In observations of the nightside with exposure times of 8 s, the digital readout from each visible pixel is low, typically 8 or less. The digital readout is a measure of the incident photon count, but it also shows spurious instrumental effects often referred to as pattern noise. To remove the latter, the recorded spectra have to be systematically accumulated. As a rule, about one thousand 8 s spectra probing the nightglow altitudes must be accumulated before the distinct pattern of the $v' = 0$ Herzberg II progression emerges.

[12] The raw data acquired with the infrared channel are converted into radiances by means of a preflight laboratory instrument transfer function (ITF). The preflight calibration of the visible channel is less certain because calibration lamps at the shorter wavelengths of the visible spectrum are less readily available. A definitive ITF that calibrates the raw data over the entire dynamic range of the instrument has, as of yet, not been issued. An alternative approach to the calibration of the visible channel is warranted. We have produced an in-flight ITF for the visible channel by dividing the uncalibrated measured spectrum of solar light scattered by the clouds by a calculated spectrum assuming the Venusian clouds are a Lambertian reflecting surface. For the spherical albedo, we adopted the determinations by *Moroz* [1981], which are consistent with those by *Travis* [1975] and with the more recent broadband measurements by *Mallama et al.* [2006]. To remove the effects that nonhomogenous clouds may introduce in the measured scattered light, we averaged the incident and emergent

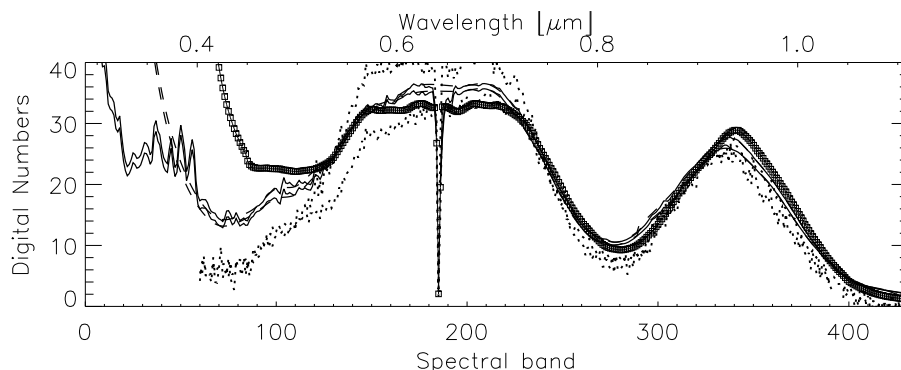


Figure 1. Empirical spectral response calibration of the visible channel of VIRTIS-M. The solid lines represent the in-flight instrument transfer function (ITF) for slit positions 102 and 150. The in-flight ITF was obtained by dividing the dayside spectrum of Venus as observed by VIRTIS by a radiative transfer model simulation which assumed the Venusian clouds behave like a Lambertian reflector with wavelength-dependent albedo from *Moroz* [1981]. The dashed lines are the corresponding spline fits for bands higher than 60, with which we have calibrated the raw VIRTIS spectra. The dashed line below band 60 is an extrapolation from the higher bands. The dotted lines is the ITF obtained from VIRTIS observations of Arcturus, also for slit positions 102 and 150. The line of square symbols is an ITF from a preflight laboratory test.

spectra from 20 orbits that span about 9 months of observations in 2007 and 2008. We have not observed a systematic variation in the resulting ITF over that period of time. To further smooth the ITF, we passed a spline fit through every tenth band (in the visible channel each band is ~ 2 nm wide) from band 60 ($\sim 0.4 \mu\text{m}$) to band 430 ($\sim 1.1 \mu\text{m}$). The radiances and other derived magnitudes presented in the work are inferred from this smoothed in-flight ITF.

[13] We tested our in-flight ITF by comparing the spectrum of Arcturus, as measured by VIRTIS, with that determined by ground-based observations. The VIRTIS spectrum of Arcturus was obtained on 2–3 December 2005, as the spacecraft cruised on its way to Venus. The star did not fill the slit, and its spectrum was recorded on only a few slit positions each day. The spectrum of this nonstandard star was revised by *Griffin and Lynas-Gray* [1999], and we followed their recommendations for wavelengths shorter than $0.86 \mu\text{m}$. Figure 1 shows as solid lines the ITF obtained from the ratio of the measured and calculated Venusian spectra for slit positions 102 and 150. Although not evident in Figure 1, the ITF varies smoothly along the slit. The spline fits are shown as dashed lines. For bands less than 60, the dashed line is an extrapolation from bands 60 and higher. The dotted lines show the ITF for the same two slit positions obtained from observations of Arcturus and scaled to match our smoothed in-flight ITF at band 340. The ITFs derived from the two methods are reasonably consistent for bands 140 and higher. We attribute the discrepancies for bands less than 140 to stray light within the instrument. This effect is well known from preflight testing. In the solar reflected spectrum, long-wavelength photons contribute artificially to the short-wavelength recorded spectrum, thus leading to the overestimation of our in-flight ITF for bands 140 and lower. This effect is minimal in the observations of the photon-starved dark side of the planet, and results in the underestimation of nighttime radiances at wavelengths shortward of $0.5 \mu\text{m}$. The low photon count in the Arcturus spectrum may also contribute

to the discrepancies. Plotted as squares is an ITF obtained in a preflight laboratory test of the instrument. The quantitative agreement with our in-flight ITF at most wavelengths is reassuring.

[14] It is apparent that for wavelengths shorter than $0.4 \mu\text{m}$ the spherical albedo cannot be represented by a continuum. The band structure in our ITF at those wavelengths is the likely result of an unaccounted for molecular absorber. Its identity will be investigated in a later study. That spectral region has no bearing on the present investigation.

2.2. The $c(0)-X(v'')$ and $A'(0)-a(v'')$ Progressions

[15] Figure 2a shows the average spectrum from 0.35 to $0.73 \mu\text{m}$ for tangent altitudes between 92 and 100 km. Bands $v'' = 4-13$ of the $v' = 0$ Herzberg II progression are readily identified. To estimate the individual band intensities, we have built synthetic spectra with the appropriate energy levels and line strength factors [*Slanger and Cosby*, 1988; *Kovacs*, 1969] in which the local continuum and relative intensity are specified by separately adjustable parameters for each band, while the spectral resolution is described by a single, band-independent parameter. An optimization algorithm determines the values for the free parameters that result in the best match to the observed spectrum. The relative band intensities inferred are listed in Table 1, along with previously published results. Our calibration seems to underestimate the relative intensity of bands $v'' < 8$, which occur at wavelengths shorter than 470 nm, but provides relative band intensities for $v'' \geq 8$ that are reasonably consistent with those published by *Lawrence et al.* [1977] and *Krasnopolsky* [1983]. These conclusions confirm the contamination of the reflected spectrum by stray photons in the derivation of our in-flight ITF. A more quantitative assessment of this phenomenon will be conducted in a later investigation. To minimize its effect, the intensities of the $c(0)-X(v'')$ progression reported hereafter are based solely on bands $v'' = 7-10$. The intensities of these four bands are summed up and corrected for with the

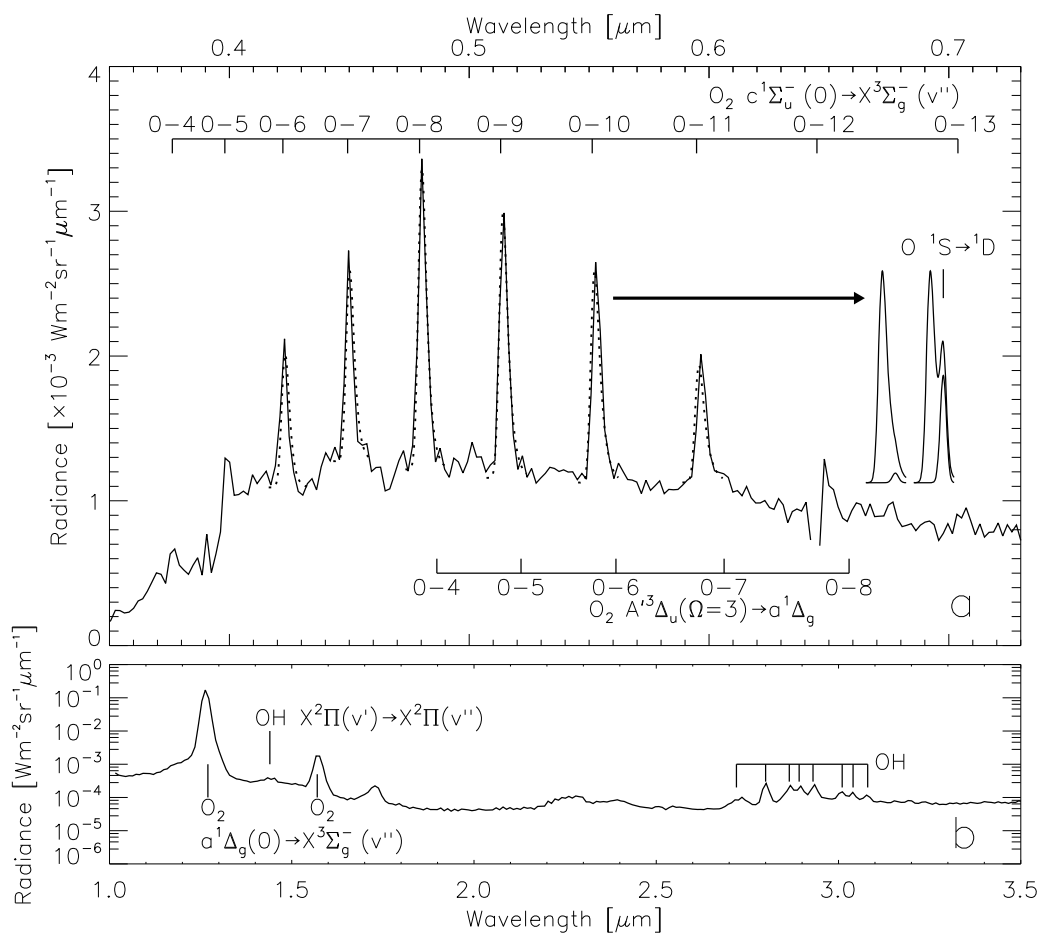


Figure 2. (a) Average visible spectrum of Venus' atmosphere for limb observations by VIRTIS with tangent altitude between 92 and 100 km. The total exposure time is about 120 h. The dotted lines are band-by-band synthetic simulations of the $c(0)-X(v'')$ progression. The summed intensity for bands $v'' = 6-11$ is 128.4 kR. For the inferred relative intensity of each band, see Table 1. The positions of the weaker $A'(0)-a(v'')$ progression for bands $v'' = 4-8$ are shown at the bottom. The separate curves to the right show the synthetic spectrum of the $c(0)-X(10)$ band that fits best the observations together with the simulation of the green line for limb-integrated intensities of 0.75 and 8.35 kR, respectively, degraded to the spectral resolution of the VIRTIS spectrum (3 nm). (b) Corresponding near-infrared spectrum. Marked are the bands from the OH Meinel and O₂ $a-X$ systems discussed by Piccioni *et al.* [2008]. Our estimated intensities for the total near-infrared O₂ and OH emissions are 29.7 MR and 590 kR, respectively. The peak at 1.74 μm and the gentle hills from 2.2 μm to 2.4 μm is thermal radiation originating from the lower atmosphere that leaks in between CO₂ absorption bands and is scattered into the line of sight of the instrument.

aid of the relative intensities calculated by Bates [1989] to determine the progression intensity. At the bottom of Figure 2a, the sticks indicate the positions of the $v' = 0$ Chamberlain progression. Our spectrum contains traces of bands $v'' = 4-8$, which were also identified by Slanger and Black [1978] in the Venera data.

[16] Figure 2b shows the corresponding near-infrared VIRTIS spectrum with the O₂ and OH Meinel bands [Piccioni *et al.*, 2008]. We infer intensities of 29.7 MR and 590 kR for the total near-infrared emissions of O₂ and OH, respectively.

2.3. Mapping of the $c(0)-X(v'')$ Progression

[17] Figure 3a shows the local time and latitude at the tangent point for our 450 h of limb-viewing observations. The data sample the evening hours more completely than

the morning hours and the northern latitudes more thoroughly than the southern latitudes. Each panel in Figure 3b displays the average spectrum from a local time/latitude region. Total exposure times and $a(0)-X(0)$ band intensities from the associated infrared spectra are given in the text insets. Short total exposure times noticeably degrade the signal-to-noise ratios of some of the spectra. Nevertheless, the $c(0)-X(v'')$ progression can be picked out in each region. Its intensity loosely correlates with that of the 1.27- μm band.

[18] The Venera observations discussed by Krasnopolsky and Tomashova [1981] mapped the $c-X$ nightglow for local times and latitudes ± 0500 h and ± 30 , respectively. Their averaged observations showed a decline in the $c-X$ intensity from the southern to the northern latitudes and a modulation in local time, with the nightglow intensity

Table 1. Relative Photon Emission Rates for the O₂ $c(0)-X(v'')$ Bands

	v''								
	5	6	7	8	9	10	11	12	13
Band origin [\AA]	3980	4222	4491	4792	5129	5510	5945	6445	7026
Lawrence <i>et al.</i> [1977] ^a	0.30	0.54	0.83	1	0.99	0.81	0.57	0.33	0.16
Lawrence <i>et al.</i> [1977] ^b	0.32	0.57	0.84	1	0.94	0.80	0.59	0.43	0.12
Krasnopolsky [1983] ^b	0.31	0.57	0.84	1	0.96	0.80	0.59	0.40	0.14
Bates [1989] ^a	0.44	0.73	0.94	1	0.85	0.60	0.35	0.18	0.07
This work		0.36	0.57	1	0.98	0.89	0.56		

^aTheory.^bExperiment.

reaching its peak shortly after midnight, passing through local minima at local times of about ± 0300 and increasing again toward ± 0500 .

[19] The maps of the visible nightglow produced by Bougher and Borucki [1994] cover local times from -0200 to 0600 and much of the low and middle latitudes

of both hemispheres. The more detailed PVO maps suggest the spatial distribution of the visible nightglow is more complex than the Venera observations found.

[20] Because of the need for long total exposure times, and the ensuing low spatial resolution of our mapping, Figure 3b, it is not possible to make direct comparison of

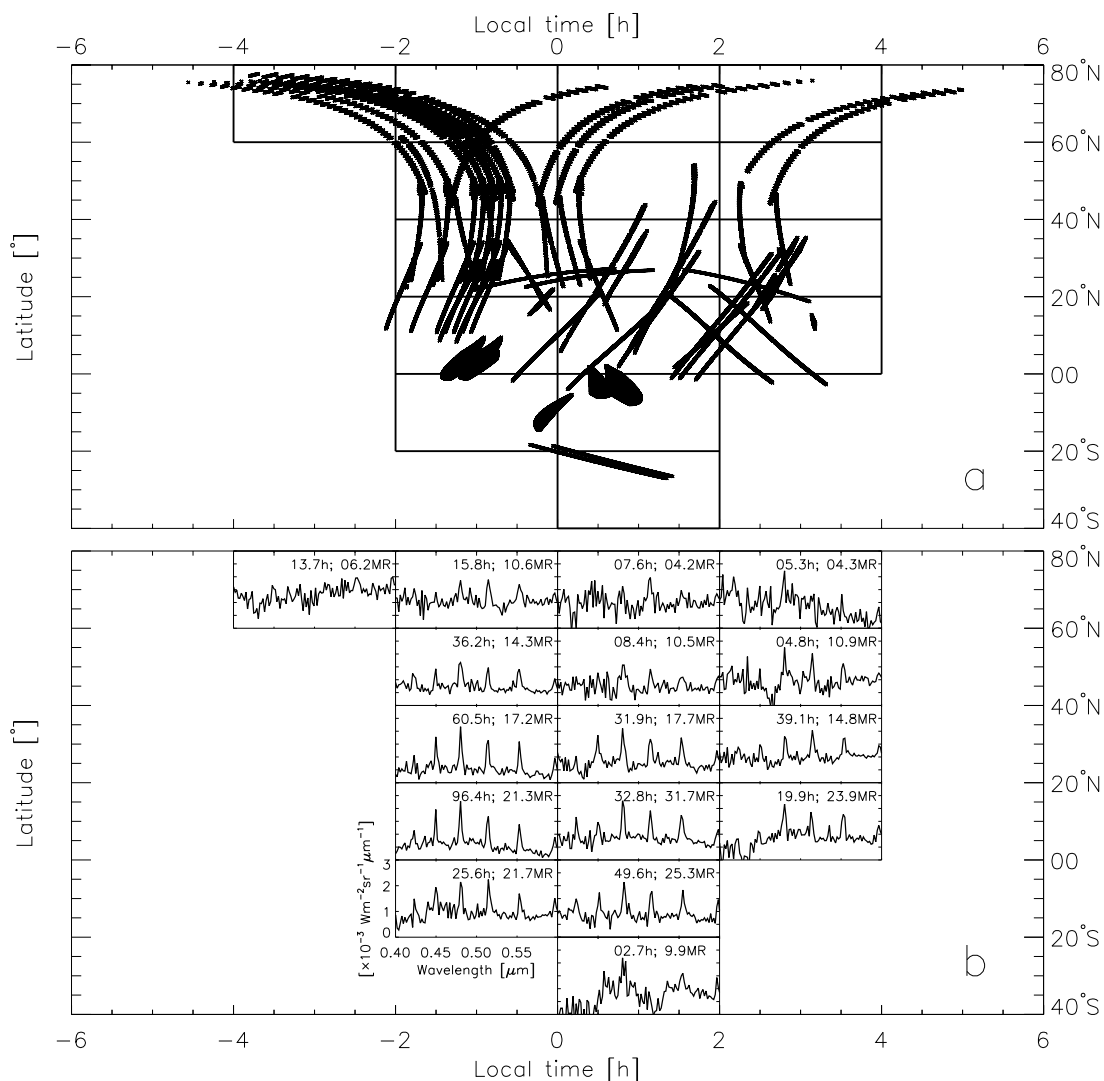


Figure 3. (a) Local time and latitude at the tangent point for the analyzed observations. (b) Average spectra from the regions indicated in Figure 3a. The total exposure time for each average spectrum and the corresponding average $a-X$ intensity are shown on each plot.

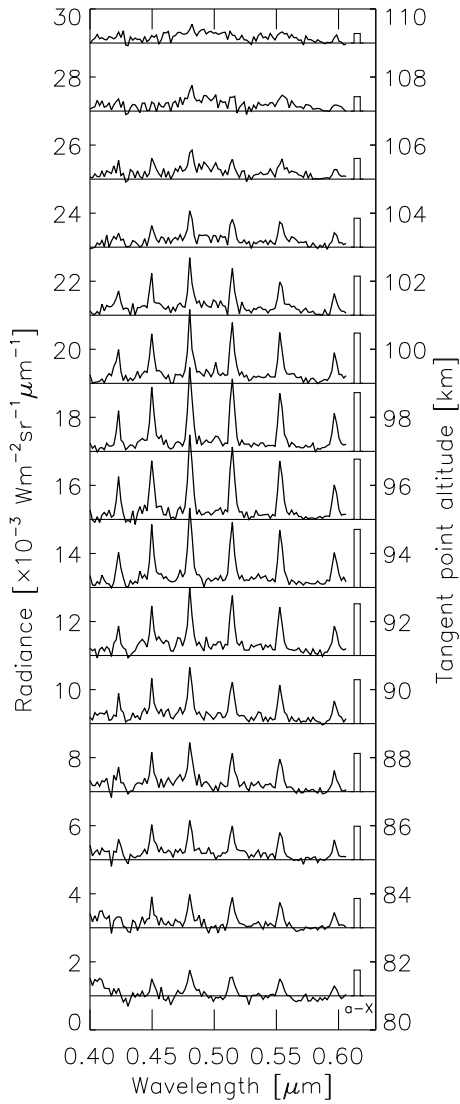


Figure 4. Spectra from all local times and all latitudes averaged over 2 km intervals for the tangent altitude from 80 km to 110 km. On the right, the corresponding $a(0)$ – $X(0)$ band intensities are shown on a linear scale. The line-of-sight $c(0)$ – $X(v'')$ and $a(0)$ – $X(0)$ intensities in the 94 km–96 km interval are 183.0 kR and 30.8 MR, respectively.

our results with the maps from the Venera and PVO missions. Significantly, all three missions have found that the visible nightglow is an ubiquitous feature.

2.4. Vertical Structure

[21] The scale height of Venus' bulk atmosphere at the nightglow altitudes is about 3.5–4 km. Thus, between 80 and 110 km the background density varies by more than 3 orders of magnitude. This is important for understanding the nightglow emission as the lifetimes of the upper states are partly dictated by collisional quenching.

[22] Figure 4 shows 15 spectra from 0.4 to 0.6 μm obtained by averaging the available data over vertical layers of 2 km height for tangent altitudes from 80 to 110 km. Each spectrum comprises about 28 h of observing time. The $c(0)$ – $X(v'')$ progression is discernible throughout the range of altitudes. To the right of each spectrum, we show the

$a(0)$ – $X(0)$ band intensity on a linear scale (in arbitrary units). It is apparent that both the c – X and a – X intensities peak near 95 km and within ± 1 km of each other. The intensities decrease more rapidly above the peak than below it due to the limb-viewing geometry. Some of the spectra show also evidence of the faint $A'(0)$ – $a(v'')$ progression.

[23] *Piccioni et al.* [2009b] have given extensive evidence of the variability in the a – X peak altitude. The peak in the average vertical profile in Figures 4 and 5 is wider than the peaks in individual vertical profiles, as expected.

3. Discussion

3.1. Definitions

[24] The accepted mechanism of formation of the O₂ nightglow in the atmospheres of the Earth and Venus is summarized by *Slanger and Copeland* [2003] as

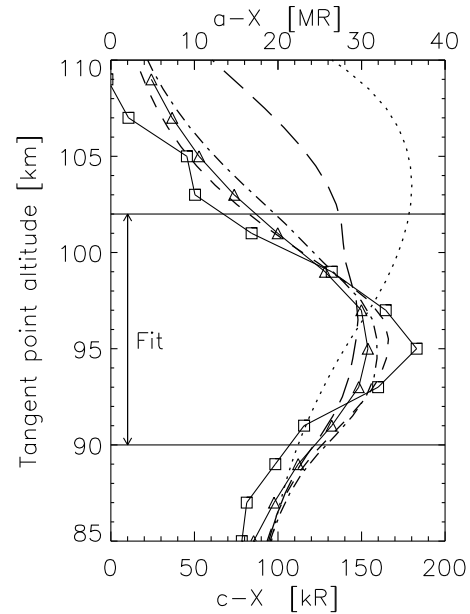
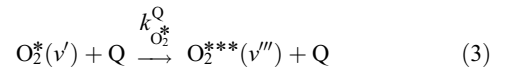
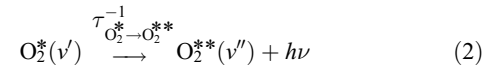
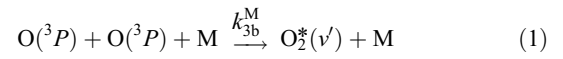


Figure 5. Line-of-sight intensity versus tangent altitude for the limb observations shown in Figure 4. Triangles, $a(0)$ – $X(0)$ band observations; squares, $c(0)$ – $X(v'')$ progression observations; dashed line, best model fit to the $c(0)$ – $X(v'')$ progression between 90 and 102 km, obtained for $\alpha_{c(0)} = 1.35 \times 10^{-2}$ and $k_{c(0)}^{\text{CO}_2} = 2.45 \times 10^{-16} \text{ cm}^3 \text{ s}^{-1}$; dotted line, model prediction of the $c(0)$ – $X(v'')$ progression based on the upper limit for $k_{c(0)}^{\text{CO}_2}$ inferred by *Kenner and Ogryzlo* [1983]; dashed-dotted line, model prediction of the $c(0)$ – $X(v'')$ progression based on the ratio $k_{c(0)}^{\text{CO}_2}/k_{c(0)}^{\text{O}_2} = 10^{-1}$; long dashed line, model prediction of the $c(0)$ – $X(v'')$ progression based on the ratio $k_{c(0)}^{\text{CO}_2}/k_{c(0)}^{\text{O}_2} = 1$ and $k_{c(0)}^{\text{CO}_2} = 0$.

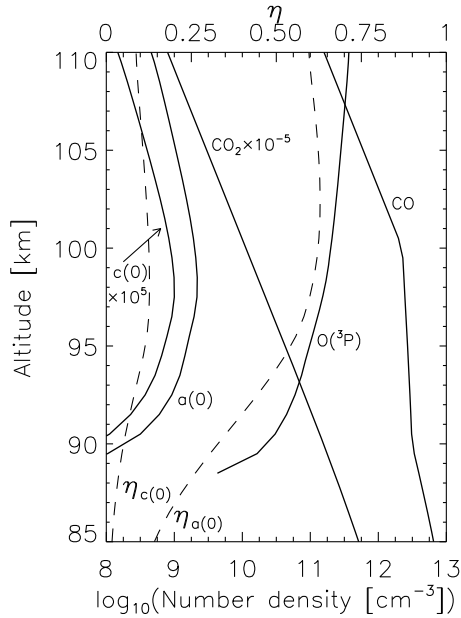


Figure 6. Profiles of atmospheric gases utilized in the model (solid lines). The CO₂ profile is from *Seiff et al.* [1985], extrapolated to 114 km following a $\log_{10}[\text{CO}_2]$ altitude law. The CO profile is from the mixing ratio profile reported by *Gurwell et al.* [1995], converted into number densities with the CO₂ profile described above. The O(³P) profile has been inferred from our a - X observations (see text). The O₂ $c(0)$ profile has been inferred from the modeling of our c - X observations (see text). Radiative efficiencies of the $a(0)$ and $c(0)$ states of O₂ (dashed lines). In either case, quenching is dominated by CO₂ and O(³P) at altitudes below and above 96 km, respectively.

In equation (1), M is a third body, typically O₂/N₂ on Earth and CO₂ on Venus. The nascent O^{*}₂ population may belong to one or more of the ⁵II, A , A' , c , b , a and X bound states that are energetically accessible, although the actual distribution is highly uncertain. O^{**}₂ and O^{***}₂ are determined, respectively, by the radiative and collisional channels open to O^{*}₂. Both vibrational and combined vibrational/electronic relaxation are possible in equations (1)–(3), which is highlighted by separate references to the vibrational quantum numbers. Equations (2) and (3) usually occur multiple times before the molecule loses its excess internal energy. This produces a population of excited O₂ with a complex distribution of energy and, consequently, a rich nightglow spectrum.

[25] In the kinetics of an excited O₂ state, one distinguishes between the production rate (or number of excited molecules produced per unit time per unit volume), $P_{\text{O}_2^*}$, the volume emission rate (or number of photons emitted during radiative relaxation into all lower states per unit time per unit volume), $V_{\text{O}_2^*}$, and the number density, $[\text{O}_2^*]$. They are related through

$$V_{\text{O}_2^*} = \tau_{\text{O}_2^*}^{-1} [\text{O}_2^*] = \eta_{\text{O}_2^*} P_{\text{O}_2^*} \quad (4)$$

where $\tau_{\text{O}_2^*}^{-1} = \sum \tau_{\text{O}_2^* \rightarrow \text{O}_2^{**}}^{-1}$ is the net transition probability, with the summation spanning all accessible lower states, and

$$\eta_{\text{O}_2^*} = \tau_{\text{O}_2^*}^{-1} / (\tau_{\text{O}_2^*}^{-1} + k_{\text{O}_2^*}^{\text{Q}_i} [\text{Q}_i]) \quad (5)$$

is the local radiative efficiency. Here, $k_{\text{O}_2^*}^{\text{Q}_i} [\text{Q}_i] = \sum k_{\text{O}_2^*}^{\text{Q}_i} [\text{Q}_i]$, with $k_{\text{O}_2^*}^{\text{Q}_i}$ being the removal rate of O^{*}₂ in collisions with the quencher Q_{*i*}. The production yield of O^{*}₂ is defined as the ratio

$$\alpha_{\text{O}_2^*} = P_{\text{O}_2^*} / P_{3b} \quad (6)$$

where

$$P_{3b} = k_{3b}^{\text{M}} [\text{O}(\text{}^3\text{P})]^2 [\text{M}] \quad (7)$$

is the recombination rate (or number of recombination events per unit time per unit volume) for equation (1). The yield is a measure of the overall production of O^{*}₂, that may occur directly through equation (1) or indirectly after relaxation from higher-energy states and, thus, is a useful parameter in the investigation of O₂ relaxation in various environments.

3.2. CO₂ and O(³P) Quenching

[26] We can utilize Figure 5 and the equations set out above to investigate the production yield and radiative efficiency of the $c(0)$ state in the nightglow. For this, we first retrieve the atomic oxygen number densities from the $a(0)$ - $X(0)$ band measurements and, second, model the $c(0)$ - $X(v'')$ progression with parameters that are either available in the literature or that we infer from the VIRTIS observations in parallel with the analysis.

[27] For the retrieval of the atomic oxygen profile, the limb-integrated $a(0)$ - $X(0)$ band intensities are converted into volume emission rates by means of a conventional onion-peeling procedure. Implicit in the onion-peeling procedure is the assumption that the nightglow layer is spherically symmetric. Equations (4)–(7) are manipulated to render a second-order polynomial in $[\text{O}(\text{}^3\text{P})]$. The polynomial is solved with the CO₂ profile for low latitudes, extrapolated to 114 km, reported by *Seiff et al.* [1985], and the relevant parameters for the $a(0)$ state, i.e., the transition probability, $2.2 \times 10^{-4} \text{ s}^{-1}$ [*Newman et al.*, 1999], and the upper limits for the quenching rates in collisions with CO₂ and O(³P), 2×10^{-20} and $2 \times 10^{-16} \text{ cm}^3 \text{ s}^{-1}$ respectively [*Sander et al.*, 2006]. We utilize the appropriate three-body recombination rate for oxygen atoms for the temperature of the nightglow in a CO₂ gas, i.e., $2.5 \times 10^{-32} \text{ cm}^6 \text{ s}^{-1}$ [*Slanger et al.*, 2006]. For the production yield, we adopt $\alpha_{a(0)} = 0.5$, which is consistent with the arguments given by *Connes et al.* [1979] and *Crisp et al.* [1996]. To the best of our knowledge, there has been no laboratory validation of such a high efficiency in the production of $a(0)$ in CO₂ other than a qualitative observation made by *Kenner and Ogryzlo* [1983]. The measured $a(0)$ - $X(0)$ limb intensities and the atomic oxygen retrieved are shown in Figures 5 and 6, respectively. Our atomic oxygen profile is generally consistent with those that *Gérard et al.* [2009] have retrieved from a few hundred VIRTIS snapshot limb measurements of the

$a(0)$ – $X(0)$ band. We note, however, that their neglect of the $a(0)$ quenching by O(³P) and their use of a higher production yield for the $a(0)$ state leads systematically to somewhat lower number densities than those reported in our work.

[28] The $a(0)$ radiative efficiency, also shown in Figure 6, is ≥ 0.5 at and above the $a(0)$ – $X(0)$ peak. As a consequence, in that range of altitudes the nightglow volume emission rates and the oxygen recombination rates exhibit similar profiles.

[29] We can proceed similarly to analyze the Herzberg II nightglow. Our model for the $c(0)$ – $X(v'')$ progression adopts the atomic oxygen profile inferred above, and the carbon dioxide profile utilized in the $a(0)$ – $X(0)$ model. Of the four parameters that are needed for the modeling of the $c(0)$ state, the transition probability has been calculated but never measured [Bates, 1989], the quenching rate in atomic oxygen has been determined from an oxygen recombination flow experiment [Kenner and Ogryzlo, 1983], only an upper limit has been inferred for the quenching rate in carbon dioxide [Kenner and Ogryzlo, 1983], and the production yield is largely uncertain.

[30] The dotted line in Figure 5 is the c – X model prediction based on the transition probability calculated by Bates [1989], 0.29 s^{-1} , and the measurement and upper limit for the $c(0)$ quenching rates in O(³P) and CO₂, 5.9×10^{-12} and $6 \times 10^{-14} \text{ cm}^3 \text{ s}^{-1}$, respectively, reported by Kenner and Ogryzlo [1983]. In this model, the c – X nightglow peaks significantly above the observations, represented in squares in Figure 5. This indicates that the Kenner and Ogryzlo [1983] upper limit for the quenching rate in CO₂ is exceedingly high and must be revised.

[31] The occurrence of the observed a – X and c – X peaks at a common altitude suggests that the ratio of radiative efficiencies $\eta_{a(0)}/\eta_{c(0)}$ remains nearly constant at the altitudes of the nightglow. This has implications for the identity of the quenchers and their quenching rates. We have adjusted both the production yield and the quenching rate in CO₂ in our model to fit the line-of-sight observations from 90 to 102 km, thus obtaining $\alpha_{c(0)} = 1.35 \times 10^{-2}$ and $k_{c(0)}^{\text{CO}_2} = 2.45 \times 10^{-16} \text{ cm}^3 \text{ s}^{-1}$. The dashed line in Figure 5 shows the line-of-sight intensities calculated based on the c – X model fit. If the CO₂ quenching rate is a factor of two smaller or larger, the modeled intensities peak about 1 km lower or higher, respectively. Thus, we estimate that the quenching rate lies in the range 1.22×10^{-16} – $4.90 \times 10^{-16} \text{ cm}^3 \text{ s}^{-1}$, with $2.45 \times 10^{-16} \text{ cm}^3 \text{ s}^{-1}$ being the best estimate. The latter conclusions, largely based on the $\eta_{a(0)}/\eta_{c(0)}$ ratio, are not strongly dependent on the profile of atomic oxygen and, consequently, on the approximations needed for its retrieval.

[32] The quenching rate inferred is 200-fold smaller than the experimental upper limit. This small rate implies that the $c(0)$ state is effectively quenched by carbon dioxide and atomic oxygen below and above 96 km, respectively. The $c(0)$ radiative efficiency in this model, Figure 6, lies in the range of 0.05–0.1 over most of the nightglow layer. It is worth noting that these details are sensitive to the precise $c(0)$ quenching rate in collisions with O(³P) adopted in the model. Lower $k_{c(0)}^{\text{O}}$ rates would lead to lower estimates of $k_{c(0)}^{\text{CO}_2}$ and $\alpha_{c(0)}$, and vice versa. The Kenner and Ogryzlo [1983] [1983] $c(0)$ quenching rate in O(³P) was obtained at

ambient temperature in a flowing afterglow experiment. It is plausible that contamination from unobserved higher-energy states could have led to an erroneous determination. A confirmation of this value and a measurement at the temperatures of the nightglow is highly desirable.

[33] In the analysis, we have thus far neglected $c(0)$ quenching by molecules such as O₂, N₂ and CO. The quenching rate in collisions with molecular oxygen has been measured by Kenner and Ogryzlo [1983]. There are no determinations of the abundance of molecular oxygen in Venus' atmosphere, but photochemical model calculations [Mills et al., 2006; Mills and Allen, 2007] suggest this molecule cannot compete with carbon dioxide or oxygen atoms in the removal of the $c(0)$ state. The nitrogen molecule has a mixing ratio of about 4 percent and remains well mixed up to altitudes above the nightglow layer. The $c(0)$ quenching rate in N₂ has not been measured, so it is possible that the carbon dioxide rate that we have deduced above contains a molecular nitrogen contribution. In the limiting case that the CO₂ quenching rate is much smaller than $2 \times 10^{-16} \text{ cm}^3 \text{ s}^{-1}$, then an N₂ quenching rate of $6 \times 10^{-15} \text{ cm}^3 \text{ s}^{-1}$ would also explain our observations. Quenching by CO is discussed below.

3.3. CO Quenching

[34] The $c(0)$ quenching rate in carbon monoxide has also not been measured. The CO molecule has been mapped in Venus' nighttime upper atmosphere at millimeter wavelengths, showing a bulge near the equator 3–4 h from local midnight toward the morning terminator [Gurwell et al., 1995]. In the bulge, the CO mixing ratio can be as high as 10^{-3} , i.e., larger than the mixing ratio of O(³P) inferred by us from our nighttime northern hemisphere observations. Clearly, CO may contribute to the removal of the $c(0)$ state if the reaction proceeds at a fast enough rate.

[35] To explore this, we have revised our c – X nightglow model and included in the radiative efficiency a carbon monoxide term. The CO profile in the model is the 1986 nighttime average profile that appears in Figure 11 of Gurwell et al. [1995]. It is reproduced in our Figure 6 after conversion into number densities. The profile suggests that the $c(0)$ quenching by CO, if significant at all, may have some altitude-dependence, which will tend to shift the c – X emission peak above the recombination peak.

[36] The dashed-dotted line in Figure 5 is the limb intensity modeled with an adopted ratio $k_{c(0)}^{\text{CO}}/k_{c(0)}^{\text{O}} = 10^{-1}$. From fitting to the observations, we obtain $\alpha_{c(0)} = 2.00 \times 10^{-2}$ and $k_{c(0)}^{\text{CO}_2} = 1.48 \times 10^{-16} \text{ cm}^3 \text{ s}^{-1}$. The shape of the profile does not differ significantly from that without CO, and there is no obvious reason to prefer one over the other. For $k_{c(0)}^{\text{CO}}/k_{c(0)}^{\text{O}} \geq 2 \times 10^{-1}$, CO becomes the dominant quencher in the nightglow layer and largely dictates the $c(0)$ radiative efficiency. This flattens the c – X profile, in clear disagreement with the observations. The long dashed line in Figure 5 is the model prediction with $k_{c(0)}^{\text{CO}}/k_{c(0)}^{\text{O}} = 1$ and $k_{c(0)}^{\text{CO}_2} = 0$. From fitting to the observations, we obtain $\alpha_{c(0)} = 6.83 \times 10^{-2}$.

3.4. Production Yield of $c(0)$

[37] The $c(0)$ – $X(v'')$ progression is a distinct feature of Venus' nightglow that is not present on Earth. This is due to the unique way in which the relaxation of the oxygen

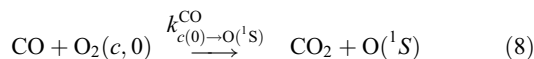
molecule occurs in carbon dioxide [Slanger, 1978]. Using the Kenner and Ogryzlo [1983] upper limit for $c(0)$ quenching in CO₂, Slanger *et al.* [2006] estimated that about 25% of recombined oxygen molecules in Venus' atmosphere end up as $c(0)$. On the contrary, our model interpretation of the VIRTIS data indicates that the percentage is only 1–2%. The moderate radiative efficiency of this state in Venus' nightglow, about 5–10%, ensures that in spite of the small production of $c(0)$, the ensuing emission is relatively intense. These $c(0)$ production yields can be compared with the yields that we infer for the $c(0)$, $A(6)$ and $A(7)$ states from a published laboratory experiment and with those inferred from terrestrial nightglow investigations. This is done in the following paragraphs.

[38] There has been no direct measurement of the production yield of excited O₂ in the recombination of oxygen atoms in carbon dioxide. From the emission measurements in a CO₂/O₂/Ar flowing afterglow experiment [Steadman and Thrush, 1994], we estimate the yields $\alpha_{A(6)} = 0.51 - 0.83$ and $\alpha_{A(7)} = 0.25 - 0.27$, which are weakly sensitive to the amount of CO₂ in the experiment. The details of our calculation are given in Appendix A. Slanger and Copeland [2003] estimate that in the terrestrial nightglow $\alpha_{A(7)} \sim 0.15$. From the data utilized by these authors, we infer a similar value for $\alpha_{A(6)}$. These yields are smaller but on the order of those obtained from our interpretation of the Steadman and Thrush [1994] experiment. It is difficult to identify the precise source of the difference, but for the present purpose it is fair to see them as reasonably consistent. In Venus' atmosphere, if we accept the production yields inferred herein from the Steadman and Thrush [1994] experiment, the abundances of the $A(6)$ and $A(7)$ states would peak at about a common altitude of 107 km and would result in limb $A(6)-X(v'')$ and $A(7)-X(v'')$ progression intensities of about 20 and 10 kR, respectively.

[39] Unlike the $v' = 6$ and 7 levels of the A state, the $c(0)$ state in the Steadman and Thrush [1994] experiment is produced above the detection threshold of their apparatus only when CO₂ is added. From the Steadman and Thrush [1994] experiment with 10% total pressure of added CO₂, we infer a production yield $\alpha_{c(0)} = 5.3 \times 10^{-2}$, which is larger than but not necessarily inconsistent with the yield deduced from the VIRTIS observations.

3.5. Green Line

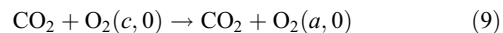
[40] The green line of atomic oxygen has been known in Venus' atmosphere for less than a decade [Slanger *et al.*, 2001]. The manner in which 4.2 eV are transferred to the excited O(¹S) atom is uncertain. The Barth mechanism (see Appendix A), with a precursor of energy equal to or higher than that of O₂($c, v = 2$), could possibly excite the green line. This is the preferred mechanism to explain the terrestrial green line. Slanger *et al.* [2006] have argued that the reaction



could be another such mechanism in Venus' atmosphere.

[41] In our earlier analysis, we have placed an upper limit of $1.2 \times 10^{-12} \text{ cm}^3 \text{ s}^{-1}$ for the rate of equation (8).

Following Slanger *et al.* [2006], this reaction might compete with



in the removal of $c(0)$, which would result in an anticorrelation between the green line and the 1.27 μm emission. Further assessment of these processes requires quantitative details on their kinetic rates and branching ratios which have not been measured yet.

[42] The ground-based observations of the green line have made it clear that its emission is highly variable. This is, in principle, not surprising as the O₂ and NO nightglows are also very variable. The green line was absent from the spectra recorded by the Venera missions. In the 1999 discovery observation, the green line was strong at about 170 R of zenith intensity. Subsequent observations have reported much fainter emissions [Slanger *et al.*, 2006].

[43] We have searched for the green line in the VIRTIS data by accumulating spectra according to altitude, local time, orbit number, or some combinations of them, in order to improve the signal-to-noise ratio of the composite spectra. We have also tentatively searched for the presumed anticorrelation between the green line and $a-X$ emissions that equations (8)–(9) suggest. Our search has not revealed any traces of the green line.

[44] If at some time during our observations there was a localized event of strong emission such as that reported by Slanger *et al.* [2001], it is conceivable that the systematic accumulation of spectra might have washed it out from the composite spectrum. In conditions of weaker emission, the green line would be practically undistinguishable from the background irregularities in the continuum of our spectra. There are, however, reasons to think that VIRTIS may detect the green line. The instrument has recently begun to be operated occasionally in limb-tracking mode, which achieves long effective exposure times over small regions. There are a few of these observations at equatorial latitudes in Figure 3a. This strategy maximizes the probability of green line detection provided that the green line is emitting strongly at the time of observing.

[45] We could, last, speculate on the reaction rate for equation (8) that would result in a green line zenith intensity of 15 R, a more typical value than the near 170 R measured in 1999 [Slanger *et al.*, 2006]. Performing the integral

$$I_{\text{zenith}}^{\text{g.l.}} = k_{c(0) \rightarrow \text{O}^1\text{S}}^{\text{CO}} \int_{90\text{km}}^{110\text{km}} \eta_{\text{O}^1\text{S}} [\text{O}_2(c, 0)] [\text{CO}] dz$$

with $\tau_{\text{O}^1\text{S}}^{-1} = 1.28 \text{ s}^{-1}$ [Kernahan and Pang, 1975] and $k_{\text{O}^1\text{S}}^{\text{CO}} = 4 \times 10^{-14} \text{ cm}^3 \text{ s}^{-1}$ [Atkinson and Welge, 1972] in $\eta_{\text{O}^1\text{S}}$, and the $c(0)$ and CO profiles from Figure 6, we obtain $k_{c(0) \rightarrow \text{O}^1\text{S}}^{\text{CO}} = 3.3 \times 10^{-14} \text{ cm}^3 \text{ s}^{-1}$. This value is appropriate at the temperature of the nightglow, i.e., about 200 K. Slanger *et al.* [2006] have argued that rate coefficients of this order for an exothermic reaction without spin restrictions are plausible. If equation (8) effectively takes place as written, and has a rate coefficient near the upper limit we have inferred, $1.2 \times 10^{-12} \text{ cm}^3 \text{ s}^{-1}$, then it could be a major pathway for production of carbon dioxide in Venus' atmosphere [Mills *et al.*, 2006].

Table A1. Our Interpretation of the *Steadman and Thrush* [1994] Experiment I^a

	Ar	O ₂	O(³ P)	CO ₂	O ₂ (a)	Σ ^b
			Number Densities [cm ⁻³]			
	2.8(17)	1(16)	5.6(14)	2.8(16)	8.0(13) ^c	
			Recombination Rate Coefficients, k_{3b}^M [cm ⁶ s ⁻¹] ^d			
	1.1(-33)	2.2(-33)	-	5.1(-33)	-	
			Recombination Rates, $k_{3b}^M[O(^3P)]^2[M]$ [cm ⁻³ s ⁻¹]			
	9.7(13)	6.9(12)	-	4.5(13)	-	1.0(14)/1.5(14)
			Removal Rate Coefficients, $k_{O_2}^{O_i}$ [cm ³ s ⁻¹] ^e			
<i>c</i> (0)	6(-16)	3(-14)	5.9(-12)	<6(-14)	6.0(-12)	
<i>A</i> (6)	1(-11)	2.8(-11)	-	7.6(-11)	-	
<i>A</i> (7)	~1(-11)	3.5(-11)	-	7.2(-11)	-	
			Removal Rates, $k_{O_2}^{O_i}$ [Q _i] [s ⁻¹]			
<i>c</i> (0)	1.7(2)	3(2)	3.3(3)	<1.7(3)	4.8(2) ^c	3.8(3)/5.5(3)
<i>A</i> (6)	2.8(6)	2.8(5)	-	2.1(6)	-	3.1(6)/5.2(6)
<i>A</i> (7)	2.8(6)	3.5(5)	-	2.0(6)	-	3.2(6)/5.2(6)

^aFor all values, we use simplified exponential notation, e.g., 6(-16) = 6 × 10⁻¹⁶.

^bThe / symbol separates values from the experiment with 0% (left) and 10% (right) added CO₂.

^cIndirect estimate, neglected in our analysis.

^d*Tsang and Hampson* [1986]. We follow *Lindner* [1988] to correct for O₂ and CO₂ as third bodies.

^e*Kenner and Ogryzlo* [1983] and *Huestis* [2002].

[46] To the right of Figure 2a we show the simulation of the *c*(0)–*X*(10) band that fits best the VIRTIS spectrum together with simulations of the green line for limb intensities of 0.75 and 8.35 kR, respectively, that correspond to zenith intensities of 15 and 167 R. For limb intensities of less than 1–1.5 kR, the green line blends smoothly with the molecular oxygen band. Thus, we place the upper limit for nondetection of the green line in our spectrum of Figure 2a at 1–1.5 kR.

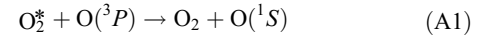
4. Conclusion

[47] We have obtained simultaneous visible and near-infrared spectra of Venus' upper atmospheric nightglow. In the visible, we observe the *c*(0)–*X*(*v*') and *A*'(0)–*a*(*v*') progressions of O₂ with the same level of detail as first seen by the Venera missions. In the near infrared, we find the O₂ and OH bands that have been described in a recent paper. Detection of the visible nightglow is beyond the nominal specifications of the instrument, so we had to accumulate hours of observations to bring the signal-to-noise ratio to acceptable levels. As a consequence, our measurements of the *c*(0)–*X*(*v*') progression have limited spatial resolution. Both the visible and near-infrared O₂ emissions exhibit a common vertical trend, which constrains the identity and removal rates of the *c*(0) quenchers. We can reproduce the observed *c*–*X* nightglow profile with a simple model in which the *c*(0) state is quenched preferentially by CO₂ and O(³P) at altitudes below and above 96 km, respectively. The *c*(0) quenching rate in collisions with CO₂ is a by-product of the model fit, and we estimate its value to be ~2.45 × 10⁻¹⁶ cm³ s⁻¹, i.e., a factor of 200 smaller than the upper limit inferred by *Kenner and Ogryzlo* [1983]. The estimated net production yield of *c*(0) is small, ~1–2% of the total recombination rate of oxygen atoms. The CO molecule may also quench the *c*(0) state, although it is unlikely that CO is the major quencher throughout the nightglow layer. We do not detect the green line of atomic oxygen at 557.7 nm. This is not unexpected as the Venera missions also failed to observe it, thus confirming that on

average the green line is much fainter than reported on the occasion of its discovery.

Appendix A: Some Comments on the *Steadman and Thrush* [1994] Work

[48] In the postulated Barth mechanism for production of the O(¹S→¹D) green line at 557.7 nm in the terrestrial atmosphere



an excited form of molecular oxygen, the precursor O₂^{*}, mediates between the recombination of oxygen atoms and the creation of O(¹S). Provided that in the controlled conditions of an experiment the Barth mechanism is the only process leading to O(¹S), the addition of a chemically nonreactive gas necessarily quenches the green line more strongly than the emission from the precursor O₂^{*}. *Stott and*

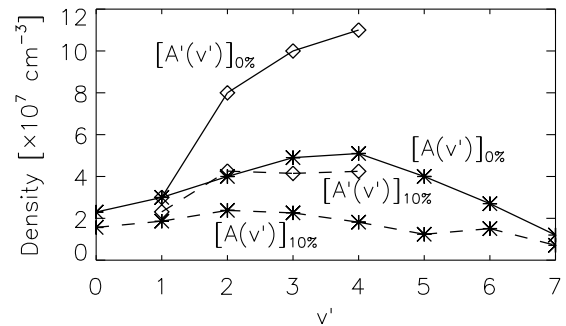


Figure A1. Number densities of the *A*(*v*' = 0–7) and *A*'(*v*' = 1–4) vibronic states of O₂ in the CO₂/O₂/Ar flowing afterglow experiments by *Steadman and Thrush* [1994]. Densities with no CO₂ added (solid lines). Densities with CO₂ added at about 10% total pressure (dashed lines), i.e., ~2.8 × 10¹⁶ cm⁻³, which is the total number density at 88 km in Venus' atmosphere.

Table A2. Our Interpretation of the *Steadman and Thrush* [1994] Experiment II

	$\tau_{O_2^*}^{-1}$ [s ⁻¹] ^a	V_{O_2} [ph cm ⁻³ s ⁻¹] ^b	η_{O_2} ^b	P_{O_2} [cm ⁻³ s ⁻¹] ^b	α_{O_2} ^b
<i>c</i> (0)	0.29	-/6.1(8)	7.7(-5)/5.3(-5)-7.7(-5) ^c	-/7.9(12)-1.2(13) ^c	-/5.3(-2)-8.0(-2) ^c
<i>A</i> (6)	11.1	3.0(8)/1.6(8)	3.6(-6)/2.1(-6)	8.3(13)/7.6(13)	8.3(-1)/5.1(-1)
<i>A</i> (7)	10.4	1.2(8)/8.0(7)	3.3(-6)/2.0(-6)	2.5(13)/4(13)	2.5(-1)/2.7(-1)

^aBates [1989] and Slinger and Copeland [2003].

^bThe / symbol separates values from the experiment with 0% (left) and 10% (right) added CO₂.

^cWe explore the entire range $k_{c(0)}^{CO_2} = 0-6 \times 10^{-14}$ cm³ s⁻¹. With the removal rate deduced from VIRTIS data, one obtains values nearly identical to those underlined.

Thrush [1989] and *Steadman and Thrush* [1994] have utilized this argument to investigate the excitation of the green line in oxygen afterglow experiments. In an O₂/Ar discharged flow where the O(³P) atoms recombine, they measured the band intensities from a few vibronic O₂ states and the intensity from O(¹S→¹D) for increasingly larger amounts of various added quenchers. Candidate precursors are identified from the ratio of intensities from the green line and the vibronic O₂ states identified in the spectra.

[49] Alternatively, those experiments can be used to draw a few conclusions on the net production yields of excited O₂. Obviously, their experiment with added CO₂ is of particular interest in the interpretation of Venus' nightglow. Table A1 summarizes the conditions in two of the *Steadman and Thrush* [1994] experiments (with/without added CO₂) and the relevant kinetic rate coefficients for their interpretation.

[50] The *A*(*v*'=0-7) and *A*'(*v*'=1-4) densities deduced by the authors (from their Figure 2) in their O₂/Ar experiment are shown in solid trace in Figure A1. The densities with CO₂ added downstream of the discharge are calculated by means of the Stern-Volmer formula

$$[O_2^*]_0/[O_2^*] = 1 + \beta[CO_2] \quad (A2)$$

and are reproduced in dashed in Figure A1. Here, β are the empirical factors listed in Table A1 of *Steadman and Thrush* [1994]. The authors could not detect *c*(0) in their O₂/Ar experiment. For their CO₂/O₂/Ar experiment, with CO₂ at about 10% total pressure, i.e., about 2.8×10^{16} cm⁻³, the authors quote a *c*(0) density of 2.1×10^9 cm⁻³.

[51] Following the scheme of equations (1)–(7), it is found that about a quarter of all recombination events pass through the *A*(7) state. The proportion is of a half or more for *A*(6). The addition of CO₂ does not alter significantly the net production yields for these two states. The lack of measurements for the removal rate coefficient of *A*(*v*' < 6) and of all *v*' levels of *A*' prevents their detailed analysis. The elevated abundances of *A*(*v*' < 6) seen in Figure A1 suggest, however, similarly high net production yields for some, if not all, of them. This argument could be extended to the *A*' state, for which densities are also elevated.

[52] Using the removal rate coefficient in collisions with O(³P) and the value in collisions with CO₂ deduced by us from the VIRTIS data, the analysis of the *c*(0) state leads to the conclusion that in the *Steadman and Thrush* [1994] experiment this state is largely quenched by O(³P) rather than Ar or CO₂ despite the small amounts of the oxygen atom produced in the discharge. The net production yield for *c*(0) inferred from the experiment with added CO₂ is 0.05. Our elaboration on the production rates, emission rates

and radiative efficiencies of the *A*(6), *A*(7) and *c*(0) states is summarized in Table A2.

[53] **Acknowledgments.** We thank ESA, ASI, CNES, and the other national agencies for their support and the members of the Venus Express team for their assistance. This work was supported by the Australian Research Council Discovery Projects grant DP0559065. The writing of the manuscript was completed at the Instituto de Astrofísica de Canarias. A. García Muñoz expresses his gratitude for the time and means offered by the IAC. Finally, we thank the two anonymous referees for their comments.

References

- Atkinson, R., and K. H. Welge (1972), Temperature dependence of O(¹S) deactivation by CO₂, O₂, N₂, and Ar, *J. Chem. Phys.*, *57*, 3689–3693.
- Bailey, J., S. Chamberlain, D. Crisp, and V. S. Meadows (2008a), Near-infrared imaging spectroscopy of Venus with the Anglo-Australian telescope, *Planet. Space Sci.*, *56*, 1385–1390.
- Bailey, J., V. S. Meadows, S. Chamberlain, and D. Crisp (2008b), The temperature of the Venus mesosphere from O₂ (*a*¹Δ_g) airglow observations, *Icarus*, *197*, 247–259.
- Bates, D. R. (1989), Oxygen band system transition arrays, *Planet. Space Sci.*, *37*, 881–887.
- Bougher, S. W., and W. J. Borucki (1994), Venus O₂ visible and IR nightglow: Implications for lower thermosphere dynamics and chemistry, *J. Geophys. Res.*, *99*, 3759–3776.
- Connes, P., J. F. Noxon, W. A. Traub, and P. Carleton (1979), O₂(¹Δ) emission in the day and night airglow of Venus, *Astrophys. J.*, *233*, L29–L32.
- Cosby, P. C., B. D. Sharpee, T. G. Slinger, D. L. Huestis, and R. W. Hueschik (2006), High-resolution terrestrial nightglow emission line atlas from UVES/VLT: Positions, intensities, and identifications for 2808 lines at 314–1043 nm, *J. Geophys. Res.*, *111*, A12307, doi:10.1029/2006JA012023.
- Crisp, D., V. S. Meadows, B. Bézard, C. de Bergh, J.-P. Maillard, and F. P. Mills (1996), Ground-based near-infrared observations of the Venus nightside: 1.27-μm O₂(*a*¹Δ_g) airglow from the upper atmosphere, *J. Geophys. Res.*, *101*, 4577–4593.
- Drossart, P., et al. (1993), Search for spatial variations of the H₂O abundance in the lower atmosphere of Venus from NIMS-Galileo, *Planet. Space Sci.*, *41*, 495–504.
- Feldman, P. D., H. W. Moos, J. T. Clarke, and A. L. Lane (1979), Identification of the UV nightglow from Venus, *Nature*, *279*, 221–222.
- García Muñoz, A., F. P. Mills, G. Piccioni, and P. Drossart (2009), The near-infrared nitric oxide nightglow in the upper atmosphere of Venus, *Proc. Natl. Acad. Sci. U. S. A.*, *106*, 985–988.
- Gérard, J.-C., A. Saglam, G. Piccioni, P. Drossart, F. Montmessin, and J.-L. Bertaux (2009), Atomic oxygen distribution in the Venus mesosphere from observations of O₂ infrared airglow by VIRTIS-Venus Express, *Icarus*, *199*, 264–272.
- Griffin, R. E. M., and A. E. Lynas-Gray (1999), The effective temperature of Arcturus, *Astrophys. J.*, *117*, 2998–3006.
- Gurwell, M. A., D. O. Muhleman, K. P. Shah, G. L. Berge, D. J. Rudy, and A. W. Grossman (1995), Observations of the CO bulge on Venus and implications for mesospheric winds, *J. Geophys. Res.*, *115*, 141–158.
- Huestis, D. L. (2002), Current laboratory experiments for planetary aeronomy, in *Atmospheres in the Solar System: Comparative Aeronomy*, *Geophys. Monogr. Ser.*, vol. 130, edited by M. Mendillo, A. Nagy, and J. H. Waite, pp. 245–258, AGU, Washington, D. C.
- Kenner, R. D., and E. A. Ogryzlo (1983), Quenching of O₂(*c*¹Σ_u⁻)*v* = 0 by O(³P), O₂(*a*¹Δ_g), and other gases, *Can. J. Chem.*, *61*, 921–926.
- Kenner, R. D., E. A. Ogryzlo, and S. Turley (1979), On the excitation of the night airglow on Earth, Venus and Mars, *J. Photochem.*, *10*, 199–204.
- Kernahan, J. A., and P. H.-L. Pang (1975), Experimental determination of absolute A coefficients for “forbidden” atomic oxygen lines, *Can. J. Phys.*, *53*, 455–458.

- Kovaacs, I. (1969), *Rotational Structure in the Spectra of Diatomic Molecules*, Elsevier, New York.
- Krasnopolsky, V. A. (1983), Venus spectroscopy in the 3000–8000 Å region by Veneras 9 and 10, in *Venus*, edited by D. M. Hunten et al., pp. 459–483, Univ. of Ariz. Press, Tucson.
- Krasnopolsky, V. A., and G. V. Tomashova (1981), Variations in the nighttime emission of Venus, *Cosmic Res., Engl. Transl.*, *18*, 556–562.
- Krasnopolsky, V. A., A. A. Krysko, V. N. Rogachev, and V. A. Parshev (1977), Spectroscopy of the night-sky luminiscence of Venus from the interplanetary spacecraft Venera 9 and Venera 10, *Cosmic Res., Engl. Transl.*, *14*, 687–692.
- Lawrence, G. M., C. A. Barth, and V. Argabright (1977), Excitation of the Venus night airglow, *Science*, *195*, 573–574.
- Lindner, B. L. (1988), Ozone on Mars: The effects of clouds and airborne dust, *Planet. Space Sci.*, *36*, 125–144.
- Mallama, A., D. Wang, and R. A. Howard (2006), Venus phase function and forward scattering from H₂SO₄, *Icarus*, *182*, 10–22.
- Mills, F. P., and M. Allen (2007), A review of selected issues concerning the chemistry in Venus' middle atmosphere, *Planet. Space Sci.*, *55*, 1729–1740.
- Mills, F. P., M. Sundaram, T. G. Slanger, M. Allen, and Y. L. Yung (2006), Oxygen chemistry in the Venus middle atmosphere, in *Advances in Geoscience*, vol. 3, *Planetary Science*, edited by W.-H. Ip and A. Bhardwaj, pp. 109–117, World Sci., Singapore.
- Moroz, V. I. (1981), The atmosphere of Venus, *Space Sci. Rev.*, *29*, 3–127.
- Newman, S. M., I. C. Lane, A. J. Orr-Ewing, D. A. Newnham, and J. Ballard (1999), Integrated absorption intensity and Einstein coefficients for the O₂ $a^1\Delta_g - X^2\Sigma_g^-$ (0, 0) transition: A comparison of cavity ringdown and high resolution Fourier transform spectroscopy with a long-path absorption cell, *J. Chem. Phys.*, *110*, 10,749–10,757.
- Ohtsuki, S., N. Iwagami, H. Sagawa, Y. Kasaba, M. Ueno, and T. Imamura (2005), Ground-based observation of the Venus 1.27- μm O₂ airglow, *Adv. Space Res.*, *36*, 2038–2042.
- Ohtsuki, S., N. Iwagami, H. Sagawa, M. Ueno, Y. Kasaba, T. Imamura, and E. Nishihara (2008a), Imaging spectroscopy of the Venus 1.27- μm O₂ airglow with ground-based telescopes, *Adv. Space Res.*, *41*, 1375–1380.
- Ohtsuki, S., N. Iwagami, H. Sagawa, M. Ueno, Y. Kasaba, T. Imamura, K. Yanagisawa, and E. Nishihara (2008b), Distributions of the Venus 1.27- μm O₂ airglow and rotational temperature, *Planet. Space Sci.*, *56*, 1391–1398.
- Piccioni, G., et al. (2008), First detection of hydroxyl in the atmosphere of Venus, *Astron. Astrophys.*, *483*, L29–L33.
- Piccioni, G., et al. (2009a), VIRTIS: The Visible and Infrared Thermal Imaging Spectrometer, *Eur. Space Agency Spec. Publ.*, *ESA-SP 1295*, Noordwijk, Netherlands, in press.
- Piccioni, G., L. Zasova, A. Migliorini, P. Drossart, A. Shakun, A. García Muñoz, F. P. Mills, and A. Cardesin-Moinelo (2009b), Near-IR oxygen nightglow observed by VIRTIS in the Venus upper atmosphere, *J. Geophys. Res.*, *114*, E00B38, doi:10.1029/2008JE003133.
- Sander, S. P., et al. (2006), Chemical kinetics and photochemical data for use in atmospheric studies, *NASA Eval. 15*, Jet Propul. Lab., Pasadena, Calif.
- Seiff, A., J. T. Schofield, A. J. Kliore, F. W. Taylor, S. S. Limaye, H. E. Revercomb, L. A. Sromovsky, V. V. Kerzhanovich, V. I. Moroz, and M. Ya. Maroc (1985), Models of the structure of the atmosphere of Venus from the surface to 100 kilometers altitude, *Adv. Space Res.*, *5*, 3–58.
- Slanger, T. G. (1978), Generation of O₂($c^1\Sigma_u^-$, $C^3\Delta_u$, $A^3\Sigma_u^+$) from oxygen atom recombination, *J. Chem. Phys.*, *69*, 4779–4791.
- Slanger, T. G., and G. Black (1978), The O₂($C^3\Delta_u \rightarrow a^1\Delta_g$) bands in the nightglow spectrum of Venus, *Geophys. Res. Lett.*, *5*, 947–948.
- Slanger, T. G., and R. A. Copeland (2003), Energetic oxygen in the upper atmosphere and the laboratory, *Chem. Rev.*, *103*, 4731–4765.
- Slanger, T. G., and P. C. Cosby (1988), O₂ spectroscopy below 5.1 eV, *J. Phys. Chem.*, *92*, 267–282.
- Slanger, T. G., P. C. Cosby, D. L. Huestis, and T. A. Bida (2001), Discovery of the atomic oxygen green line in the Venus night airglow, *Science*, *291*, 463–465.
- Slanger, T. G., P. C. Cosby, and D. L. Huestis (2004), Co-variation of nightglow emission from the O₂($A^3\Sigma_u^-$) and O₂($c^1\Sigma_u^-$) states and the oxygen green line, observed with the Keck I/II telescopes, *J. Atmos. Solar Terr. Phys.*, *66*, 617–622.
- Slanger, T. G., D. L. Huestis, P. C. Cosby, N. J. Chanover, and T. A. Bida (2006), The Venus nightglow: Ground-based observations and chemical mechanisms, *Icarus*, *182*, 1–9.
- Steadman, J. A., and B. A. Thrush (1994), A laboratory study of the mechanism of the oxygen airglow, *J. Atmos. Chem.*, *18*, 301–317.
- Stott, I. P., and B. A. Thrush (1989), Laboratory studies of the mechanism of the oxygen airglow, *Proc. R. Soc. London A*, *424*, 1–17.
- Travis, L. D. (1975), On the origin of ultraviolet contrasts on Venus, *J. Atmos. Sci.*, *32*, 1190–1200.
- Tsang, W., and R. F. Hampson (1986), Chemical kinetic data base for combustion chemistry. Part I. Methane and related compounds, *J. Chem. Phys. Ref. Data*, *15*, 1087–1279.

P. Drossart, LESIA, Observatoire de Paris, UPMC, Université Paris-Diderot, CNRS, 5 Place Jules Janssen, F-92195 Meudon, France.

F. P. Mills, Research School of Physics and Engineering, Australian National University, Canberra, ACT 0200, Australia.

A. García Muñoz, Instituto de Astrofísica de Canarias, Vía Láctea, E-38205 La Laguna, Tenerife, Spain. (agm@iac.es)

G. Piccioni, Istituto di Astrofisica Spaziale e Fisica Cosmica, Via del fosso del Cavaliere 100, I-00133 Rome, Italy.

T. G. Slanger, Molecular Physics Laboratory, SRI International, 333 Ravenswood Ave., Menlo Park, CA 94025, USA.